Pápai M, Vankó G, Rozgonyi T, Penfold T.

High-Efficiency Iron Photosensitizer Explained With Quantum Wavepacket Dynamics.

***Journal of Physical Chemistry Letters* 2016, 7, 2009-2014.**

DOI: http://dx.doi.org/10.1021/acs.jpclett.6b00711

High Efficiency Iron Photosensitiser Explained With Quantum Wavepacket Dynamics

Mátyás Pápai,[†,‡] György Vankó,[¶] Tamás Rozgonyi,[§] and Thomas J Penfold[*,‖]

†*Wigner Research Centre for Physics, Hungarian Academy of Sciences, P.O. Box 49, H-1525 Budapest, Hungary.*

‡*Department of Chemistry, Technical University of Denmark, DK-2800, Kongens Lyngby, Denmark.*

¶*Wigner Research Centre for Physics, Hungarian Academy of Sciences, P.O. Box 49, H-1525 Budapest, Hungary.*

§*Institute of Materials and Environmental Chemistry, Research Centre for Natural Sciences, Hungarian Academy of Sciences, P.O. Box 286, H-1519 Budapest, Hungary*

‖*School of Chemistry, Newcastle University, Newcastle upon Tyne, NE1 7RU, United Kingdom.*

E-mail: tom.penfold@ncl.ac.uk

Abstract

Fe(II) complexes have long been assumed unsuitable as photosensitisers because of their low-lying non-emissive metal centred (MC) states, which inhibit electron transfer. Herein, we describe the excited state relaxation of a novel Fe(II) complex that incorporates N-heterocyclic carbene ligands designed to destabilise the MC states. Using first principles quantum nuclear wavepacket simulations we achieve a detailed understanding of the photoexcited decay mechanism, demonstrating that it is dominated by an ultrafast intersystem crossing from ^{1}MLCT-^{3}MLCT proceeded by slower kinetics associated with the conversion into the ^{3}MC states. The slowest component of the ^{3}MLCT decay, important in the context of photosensitisers, are much longer than related Fe(II) complexes because the population transfer to the ^{3}MC states occurs in a region of the potential where the energy gap between the ^{3}MLCT and ^{3}MC states is large, making the population transfer inefficient.

Graphical TOC Entry

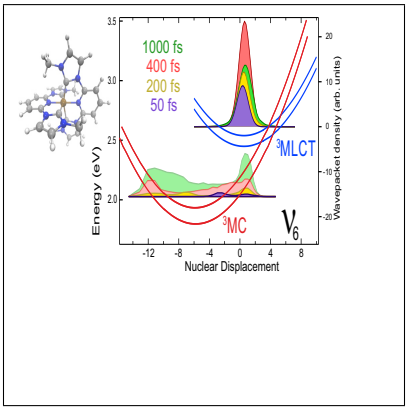

Keywords

Keywords: Fe(II)-NHC Complexes, Quantum dynamics, Vibronic Coupling, Intersystem crossing

Metal-to-ligand charge transfer (MLCT) states are at the heart of photophysical processes in transition metal complexes and, in recent years, have been extensively exploited for application as photosensitisers in photovoltaics or photocatalysts.[1,2] For this purpose complexes containing rare and often environmentally unfriendly metal centres, such as Ru(II),[3] are most widely used as their low lying valence excited states are predominantly long-lived MLCT states. Despite exhibiting an intense MLCT absorption band, the analogous Fe(II) complexes are considered unsuitable for these applications due to low lying metal centred (MC) states.[4] These contribute to an extremely rich and ultrafast dynamics culminating in the phenomenon known as light-induced excited spin-state trapping (LIESST).[5,6] The dynamics of these systems are epitomised by the excited state decay of $[Fe(bipy)_3]^{2+}$, represented schematically in Figure 1a. After excitation into the ^{1}MLCT band, this complex relaxes into the non-emissive quintet MC ($^5T_2$) state within ∼100 fs.[8,9] Importantly, this decay route makes $[Fe(bipy)_3]^{2+}$, and other related complexes,[10–12] unsuitable for applications as photosensitisers, as the MC states transfer the photoexcited electrons away from outer ligand-based regions of the complex, preventing charge transfer and/or injection.[13]

The absence of low lying MC excited states in complexes containing second and third row transition metal ions is due to their larger d-d splitting (the so-called ligand field splitting). However, this splitting also depends on the structure and bonding of the ligands, yielding the potential for Fe(II) complexes with reduced MC contribution in the lowest valence excited states. Liu *et al.*[14] demonstrated this by exploiting strongly σ-donating N-heterocyclic carbene ligands to create $[Fe(bmip)_2]^{2+}$(bmip=2,6-bis(3-methyl-imidazole-1-ylidine)pyridine) shown in Figure 1b. Using ultrafast transient absorption, the authors reported a ^{1}MLCT-^{3}MLCT conversion of ∼100 fs, no population of a high spin $^5T_2$ state and a ^{3}MLCT lifetime of ∼9 ps, which is ∼100 times longer than the MLCT lifetimes of other Fe(II) complexes. Harlang *et al.*[15] have recently exploited this long ^{3}MLCT lifetime to implement $[Fe(bmip)_2]^{2+}$as a photosensitiser attached to titanium dioxide, reporting photoelectrons in the conduction band of titanium dioxide generated by injection from the ^{3}MLCT

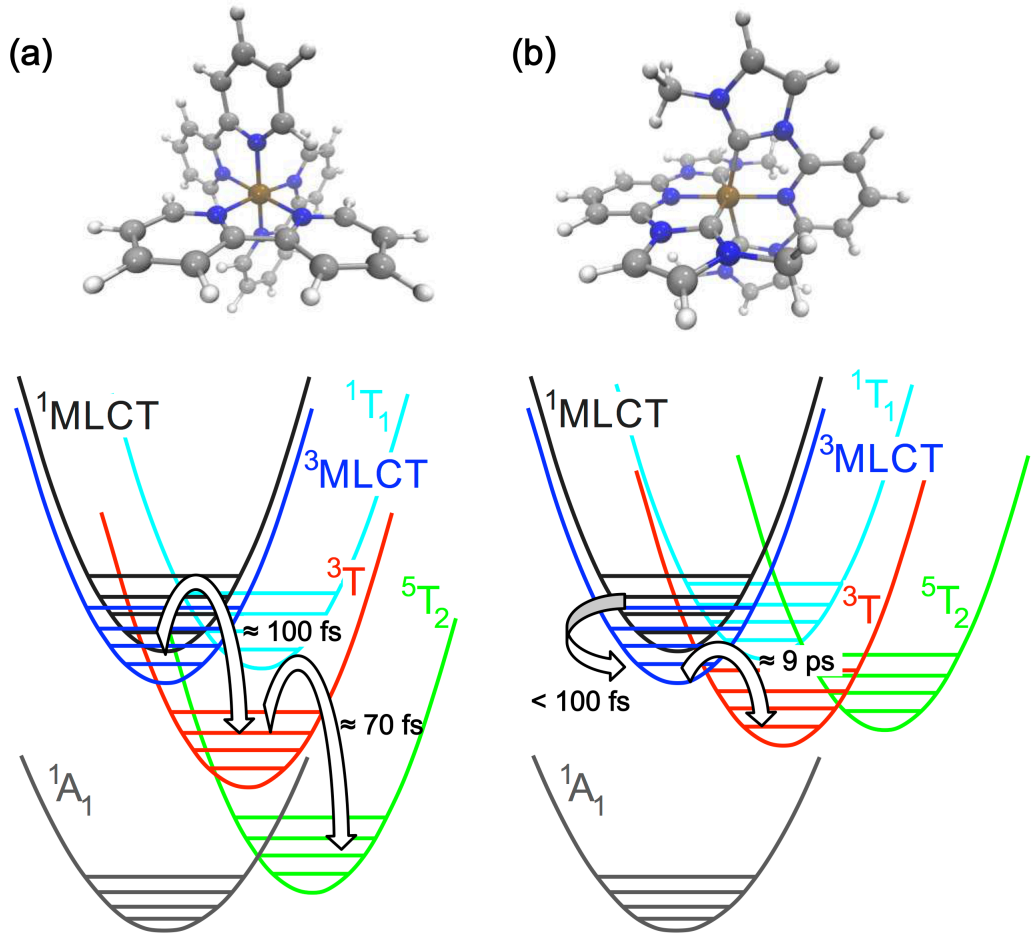

Figure 1: Schematic of the potential energy surfaces, proposed decay pathways and timescales involved in the excited state deactivation of $[Fe(bipy)_3]^{2+}$(a) and $[Fe(bmip)_2]^{2+}$(b).

state of $[Fe(bmip)_2]^{2+}$with quantum yield of 92%.

To understand the photoexcited dynamics of $[Fe(bmip)_2]^{2+}$, Fredin *et al.*[16] used unrestricted density functional theory (uDFT) and time-dependent DFT (TDDFT) to compute potential energy curves of the relevant ground and excited states. They confirmed that the bmip ligands led to destabilisation of the MC states. They also proposed that the origin of the long ^{3}MLCT lifetime was due to significant geometry reorganisation between the two states, i.e. the time required to stretch the Fe-C bonds, solvent reorientation, and thermally driven diffusion. However, the latter two variables were not included in their computations.

In addition, the structural changes in the MLCT excited states are very small, indeed in $[Fe(bipy)_3]^{2+}$similar structural changes occur within 100-200 fs.[8,9] It is therefore surprising that this population transfer from the ^{3}MLCT$\rightarrow ^3$MC occurs with a time constant as long as $\sim$9 ps. One drawback of the computations in ref.[16] is that they provide a static representation of a dynamical process. Indeed spin-orbit and nonadiabatic couplings, responsible for this conversion, are dynamical in the sense that they arise and become dominant from the system traversing regions of the potential energy surface where there is strong coupling. Consequently, such processes can only be fully addressed using a time-dependent representation, such as quantum dynamics. In this paper, we perform high level wavepacket quantum dynamics simulations that shed new insight into the important dynamics associated with the photorelaxation of $[Fe(bmip)_2]^{2+}$.

Figure 2 shows the spin-free potential energy curves along 4 normal modes (ν_6, ν_{11}, ν_{25} and ν_{36}) identified, using the magnitude of the linear coupling constants (see section S1 in the supporting material for computational details and a description of how the 4 modes were chosen), to be most important for the excited state dynamics associated with relaxation into the ^{3}MC states. Animations of these 4 normal mode vibrations are included in the supplementary material. These show that ν_6 is a totally symmetric breathing mode with symmetry, within the D_{2d} point group, of a_1, ν_{11} and ν_{25} are antisymmetric stretching modes with symmetry b_2, predominately acting on the Fe-C and Fe-N bonds, respectively. ν_{36} is another totally symmetric breathing mode with symmetry a_1, predominantly acting on the Fe-N bonds. The structural distortions along the mass-frequency scaled normal modes shown in Figure 2a and 2d correspond to symmetric changes in the Fe-N and Fe-C bond distances between the ground and ^{3}MC states of $\sim$0.1 Å, (Fe-N =1.95$\rightarrow$2.05 Å and Fe-C = 1.99$\rightarrow$ 2.07 Å). Asymmetric changes in the ^{3}MC with respect to the pseudo-octahedral symmetry arise from small distortions along ν_{11}. A full structural reorganisation to give full agreement with the optimised ^{3}MC state structure reported in ref.[16] also requires the addition of several asymmetric b_2 symmetry normal modes, including ν_{31}, ν_{39}, ν_{45} and ν_{55}. However these

modes were found to exhibit no significant nonadiabatic coupling and therefore would have no effect on the decay dynamics into the ^{3}MC. Consequently, these modes were not included in the simulations as they would cause a prohibitively large computational effort. While these modes could not be discounted for studies of longer time dynamics within the ^{3}MC, such as vibrational redistribution and relaxation to the ground state, such dynamics are beyond the scope of the present study. In contrast the MLCT states, critical in the context of the present study exhibit only minor structural changes from the ground state geometry.

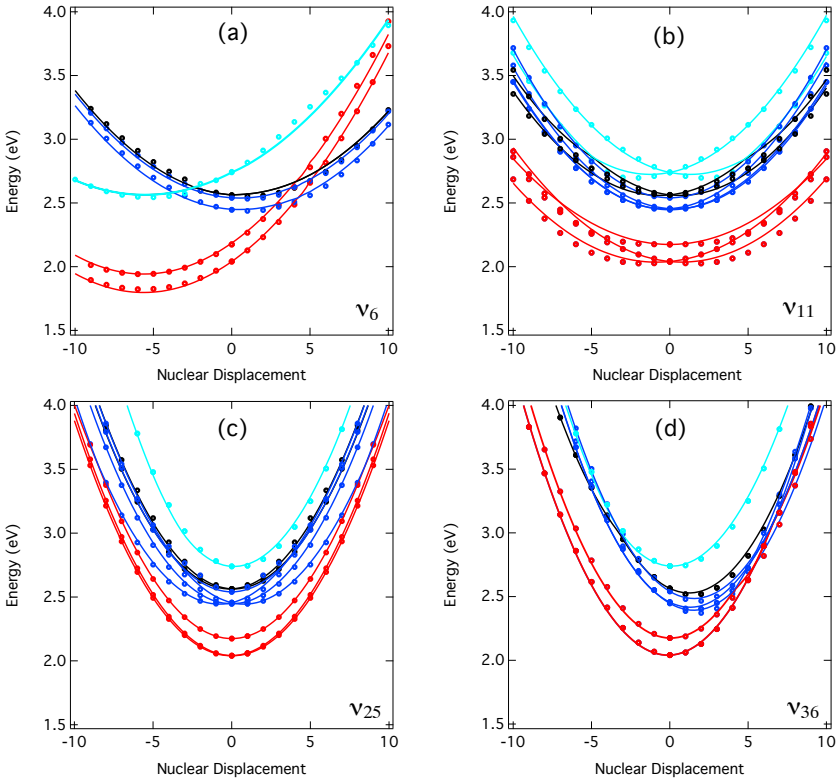

Figure 2: Cuts through the spin-free potential energy surface along (a) ν_6 , (b) ν_{11}, (c) ν_{25} and (d) ν_{36} normal modes. The dots are derived from the quantum chemistry calculations. The lines correspond to their fit from which the expansion coefficients of the diabatic Vibronic Coupling Hamiltonian are determined, see section S1 for a detailed description. Colour code is as follows: ^{1}MLCT: black, ^{3}MLCT: blue, ^{1}MC: Cyan and ^{3}MC: red.

The breathing mode, ν_6, is expected to dominate the nuclear dynamics as the lowest energy geometry of the ^{3}MC states (red lines) shows significant displacement along this mode from the lowest energy geometry of the ^{1,3}MLCT states. This is consistent with

the excited state dynamics of other Fe(II) complexes, such as $[Fe(bipy)_3]^{2+}$,[7,19] which are usually schematically represented with the vibrational motion reduced to one vibrational coordinate. However while these so called *tuning modes* are usually responsible for the largest structural distortions and therefore tend to dominate any experimental spectroscopic observable,[9] other modes, so called *coupling modes*, will usually contain the nonadiabatic coupling crucial to population transfer between excited states. The dominant *coupling modes* for $[Fe(bmip)_2]^{2+}$were found to be the antisymmetric stretching modes ν_{11} and ν_{25}. Indeed, while the minimum of each state is not displaced from the ground state minimum, and will therefore not drive strong nuclear motion, there is sizeable nonadiabatic coupling along these modes (Table S4) as demonstrated by the splitting between the singlet and triplet states that are degenerate at the Franck-Condon geometry. This is important for permitting population transfer between the different states. ν_{36}, the combined symmetric Fe-N stretching mode, exhibits a similar potential energy profile to ν_6 and consequently is classed as a *tuning mode*, driving the nuclear motion during the dynamics.

These potential curves form the spin-vibronic Hamiltonian[17,18] used during the quantum dynamics. Figure 3a shows the population kinetics of the ^{1}MLCT, ^{3}MLCT, ^{1}MC and ^{3}MC states (composed of a a total of 25 separate electronic states) following excitation into the lowest ^{1}MLCT states. The dynamics are dominated by three temporal components and weak coherent wavepacket oscillations between the ^{1}MLCT and ^{3}MLCT states. The first kinetic component is ultrafast ISC from ^{1}MLCT$\rightarrow$^{3}MLCT. Using an exponential fit to the population kinetics (Figure 3a solid black line) we find that the ^{1}MLCT$\rightarrow$^{3}MLCT dynamics has a time constant of $\sim$100 fs in excellent agreement with previous experimental observations.[14] The rapid nature of the dynamics is a result of the close energetic proximity of the ^{1}MLCT and ^{3}MLCT states. This promotes strong mixing of the two states and leads to efficient population transfer. This is highlighted in Figure 3b showing the population of the individual triplet states during the dynamics. Crucially it is the highest ^{3}MLCT (labelled $^3MLCT_4$ in Figure 3b) which is predominantly populated during the initial dynamics, as this

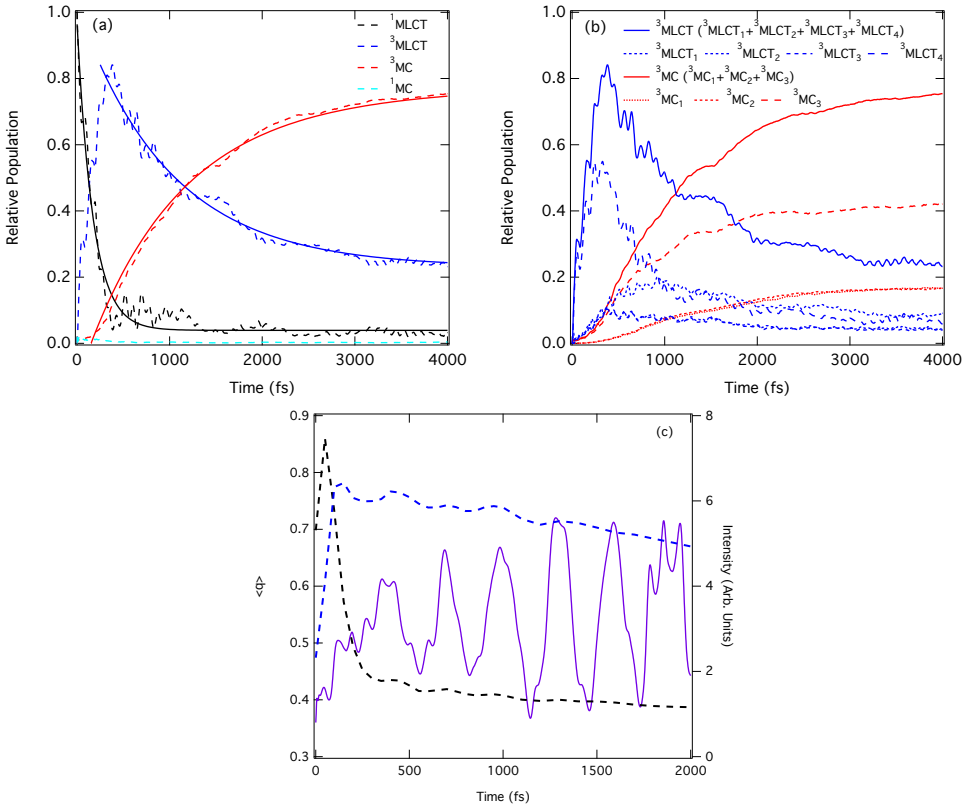

Figure 3: (a) Relative diabatic state populations of the ^{1}MLCT (black dashed), ^{3}MLCT (blue), ^{1}MC (cyan dashed) and ^{3}MC (red dashed) states for 4 ps following photoexcitation. The solid lines are exponential fits of the populations kinetics. (b) Relative diabatic state populations of each of the ^{3}MLCT (blue), and ^{3}MC (red) state during the dynamics. (c) Expectation value of the position, $\langle q \rangle$ of the wavepacket in the ^{3}MLCT state along ν_6 (purple) plotted with the transient absorption data in ref.[14] integrated between 600-680 nm (black line) 510-538 nm (blue line) corresponding to the ^{1}MLCT and ^{3}MLCT states, respectively.

state is the only ^{3}MLCT degenerate with the ^{1}MLCT states (see Table S3). Once populated, the wavepacket slowly redistributes between the other ^{3}MLCT states at times >500 fs .

Figure 3a also shows weak coherent population transfer between the ^{1}MLCT and ^{3}MLCT states with a period of ∼1 ps. Based upon the assumption of two coupled harmonic oscillators, the period of these oscillations, using the Rabi formula, is determined by the energy gap and spin-orbit coupling between the two states. Indeed, they correspond to the frequency of ∼30 cm^{-1}, similar to the magnitude of the spin-orbit coupling between the two states, with the slight discrepancy arising from the modulation of the energy gap between the two

states along ν_{11} and ν_{25}. They are observed here, and not experimentally because of the over coherence of our present model arising from the reduced nuclear coordinate space of the Hamiltonian. In terms of coherent wavepacket motion, previous experimental data[14] (Figure 3c) exhibits a weak oscillatory period closer to 300 fs. In our present simulations, this oscillatory component is very clearly observed in the wavepacket along ν_6 in the ^{3}MLCT, ^{1}MLCT and ^{3}MC states (Figure 3c purple line, Figure S2 and Figure S3, respectively). This reveals that the principal nuclear dynamics during the excited state decay are dominated by the nuclear motion along one nuclear degree of freedom, in this present case ν_6 with a period of 300 fs.

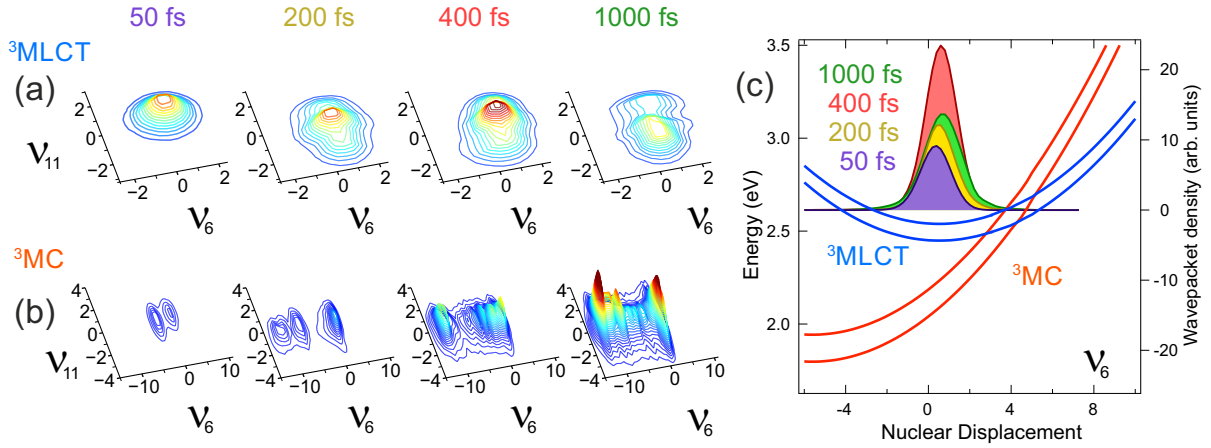

Figure 4: Snapshots of the wavepacket density in the ^{3}MLCT (a), and ^{3}MC (b) states projected along ν_6 and ν_{11} at time delays of 50, 200, and 400 and 1000 fs after photoexcitation. (c) One dimensional projection of the wavepacket in the ^{3}MLCT along ν_6 overlayed with the potential energy surface.

The second and third kinetic components are associated with the rise of the ^{3}MC population. The first has a time constant of ∼1 ps, which is followed by a slower component consistent with a time constant >4 ps in agreement with that observed experimentally.[14] Importantly, this is significantly slower than the ^{1}MLCT→^{3}MLCT transition and the 3 ps reported by Harlang *et al.*[15] for injection of photoelectrons into the conduction band of

TiO_2, supporting the conclusions of ref.[15] regarding the efficient electron transfer step crucial to dye-sensitised solar cells. This population transfer (^{3}MLCT$\rightarrow^3$MC) step is between two triplet states and therefore may occur via two mechanisms, nonadiabatic or spin-orbit coupling. Initially, when the majority of the wavepacket is in the highest ^{3}MLCT state (Figure 3b) both mechanisms contribute and this gives rise to the initial fast component of the decay dynamics. Here motion along ν_{36} also plays an important role. However after population redistribution amongst the triplet states (Figure 3b), the contribution of nonadiabatic coupling is reduced, as it is weaker for the other triplet states, as shown in Table S4. From this point spin-orbit coupling dominates. This is confirmed by Figure S1 showing the population of the ^{3}MC states using our model Hamiltonian without including nonadiabatic coupling. In this case we observe essentially the same longer dynamics, but no initial fast decay. Importantly, in agreement with the ref.[14] even though only one coupling mechanism is operational for the later time dynamics, the ^{3}MLCT to ^{3}MC conversion remains surprisingly slow. To understand this, Figure 4 shows snapshots of the nuclear wavepacket density projected along ν_6 and ν_{11} for the ^{3}MLCT and ^{3}MC states. This shows that the majority of the wavepacket on the ^{3}MLCT states resides around its energy minimum geometry. As seen in Figure 4, this region of the potential energy surface is not very close to the crossing point between the ^{3}MLCT-^{3}MC states, which exhibits displacement from the ^{3}MLCT minimum. As demonstrated using the nuclear wavepacket density plots for the ^{3}MC, the population transfer predominantly occurs away from the crossing point at or near the energy minimum geometry of the ^{3}MLCT states. Crucially, the energetic separation of the ^{3}MLCT-^{3}MC states is >0.1 eV and therefore regardless of the coupling strength, efficient population transfer is difficult. It is this dynamics, away from the crossing point of the two states which causes the slow population decay of the ^{3}MLCT state.

In summary, quantum dynamics has been used to describe the excited state deactivation mechanism of a novel Fe(II) complex, $[Fe(bmip)_2]^{2+}$. Including the dominant electronic and nuclear degrees of freedom we have obtained detailed insights into the dynamics pointing to

a clear interpretation of the ultrafast excited state decay. After photoexcitation, ultrafast ISC is observed from ^{1}MLCT$\rightarrow$^{3}MLCT within 100 fs. The driving force for this is the near degeneracy of the states, close to the Franck-Condon geometry meaning little or no nuclear motion is required to achieve the population transfer. Proceeding this, decay into the ^{3}MC states is observed. However, this is slower because the wavepacket does not readily reach the crossing between the states and therefore population transfer occurs in the region of the potential energy surface where the energy gap between the two states is large making it inefficient.

Computational Details

The potential energy surfaces were calculated using TDDFT(B3LYP*)[20] within the Tamm-Dancoff approximation (TDA)[21] and a TZVP basis set[22] as implemented within the ORCA quantum chemistry package.[24] The SOC matrix elements were computed using the perturbative approach[23] implemented within ADF.[25] The Hamiltonian used is based upon the Vibronic Coupling Hamiltonian.[26] The quantum dynamics were performed using the Heidelberg Multi Configuration Time Dependent Hartree (MCTDH) package.[27] Further details are provided in the supporting material.

Associated Content

The expansion coefficient for the vibronic coupling Hamiltonian and spin orbit couplings can be found in the supporting information. This material is available free of charge via the Internet at http://pubs.acs.org.

Acknowledgements

This project was supported by the European Research Council via contract ERC-StG-259709 (X-cited!), the 'Lendület' (Momentum) Program of the Hungarian Academy of Sciences

(LP2013-59), and the Hungarian Scientific Research Fund (OTKA) under contract K29724 and the People Programme (Marie Curie Actions) of the European Union's Seventh Framework Programme (FP7/2007-2013) under REA grant agreement number 609405 (COFUND-PostdocDTU). The authors would also like to thank Tobias Harlang for sharing the transient absorption data shown in Figure 3c.

References

(1) Hagfeldt, A. & Graetzel, M. Light-induced Redox Reactions in Nanocrystalline Systems. *Chem. Rev.* **1995**, *95*, 49–68.

(2) Youngblood, W. J., Lee, S.-H. A., Maeda, K. & Mallouk, T. E. Visible Light Water Splitting Using Dye-Sensitized Oxide Semiconductors. *Acc. Chem. Res.* **2009**, *42*, 1966–1973.

(3) Nazeeruddin, M. K. *et al.* Conversion of Light to Electricity by Cis-X2bis (2, 2'-bipyridyl-4, 4'-dicarboxylate) Ruthenium (ii) Charge-Transfer Sensitizers (X= Cl-, Br-, I-, CN-, and SCN-) on Nanocrystalline Titanium Dioxide Electrodes. *J. Am. Chem. Soc.* **1993**, *115*, 6382–6390.

(4) Hauser, A. Light-induced Spin Crossover and the High-Spin Low-Spin Relaxation. In *Spin Crossover in Transition Metal Compounds II*, 155–198 (Springer, **2004**). .

(5) Decurtins, S., Gutlich, P., Kohler, C., Spiering, H. & Hauser, A. Light-Induced Excited Spin State Trapping in a Transition-Metal Complex: The Hexa-1-Propyltetrazole-Iron (ii) Tetrafluoroborate Spin-Crossover System. *Chem. Phys. Lett.* **1984**, *105*, 1–4.

(6) Hauser, A., Vef, A. & Adler, P. Intersystem Crossing Dynamics in Fe(ii) Coordination Compounds. *J. Chem. Phys.* **1991**, *95*, 8710.

(7) Cannizzo, A. *et al.* Light-Induced Spin Crossover in Fe(II)-based Complexes: The Full

Photocycle Unraveled by Ultrafast Optical and X-ray Spectroscopies. In *Coord. Chem. Rev.*, **2010**, *254*, 2677–2686.

(8) Zhang, W. *et al.* Tracking Excited-State Charge and Spin Dynamics in Iron Coordination Complexes. *Nature* **2014**, *509*, 345–348.

(9) Auböck, G. & Chergui, M. Sub-50-fs Photoinduced Spin Crossover in [Fe(bpy)3]2+. *Nature Chem.* **2015**, *7*, 629–633.

(10) Vanko, G. *et al.* Detailed Characterization of a Nanosecond-lived Excited State: X-ray and Theoretical Investigation of the Quintet State in Photoexcited [Fe(terpy)2]2+. *J. Phys. Chem. C* **2015**, *119*, 5888–5902.

(11) Van Kuiken, B and Cho, H and Hong, K and Khalil, M and Schoenlein, RW and Kim, TK and Huse, N Time-Resolved X-ray Spectroscopy in the Water Window: Elucidating Transient Valence Charge Distributions in an Aqueous Fe (II) Complex. *J. Phys. Chem. Lett.* **2016**, *7*, 465–470.

(12) Jamula, LL and Brown, AM and Guo, D and McCusker, JK Synthesis and Characterization of a High-Symmetry Ferrous Polypyridyl Complex: Approaching the 5T2/3T1 Crossing Point for FeII. *Inorg. Chem.* **2014**, *53*, 15-17.

(13) Ardo, S. & Meyer, G. J. Photodriven Heterogeneous Charge Transfer with Transition-Metal Compounds Anchored to TiO2 Semiconductor Surfaces. *Chem. Soc Rev.* **2009**, *38*, 115–164.

(14) Liu, Y. *et al.* Towards Longer-lived Metal-to-Ligand Charge Transfer States of Iron(ii) Complexes: An N-heterocyclic Carbene Approach. *Chem. Comm.* **2013**, *49*, 641249, 6412 (2013). .

(15) Harlang, T. C. B. *et al.* Iron Sensitizer Converts Light to Electrons with 92% Yield. *Nature Chem.* **2015**, *7*, 883–889.

(16) Fredin, L. A. *et al.* Exceptional Excited-State Lifetime of an Iron(II)– N-Heterocyclic Carbene Complex Explained. *J. Phys. Chem. Lett.* **2014**, *5*, 2066–2071.

(17) Capano, G., Chergui, M., Rothlisberger, U., Tavernelli, I. & Penfold, T. J. A Quantum Dynamics Study of the Ultrafast Relaxation in a Prototypical Cu(i)-phenanthroline. *J. Phys. Chem. A* **2014**, *118*, 9861.

(18) Eng, J., Gourlaouen, C., Gindensperger, E. & Daniel, C. Spin-vibronic Quantum Dynamics for Ultrafast Excited-State Processes. *Acc. Chem. Res.* **2015**, *48*, 809–817.

(19) Hauser, A. Intersystem Crossing in the [Fe(ptz)6](bf4)2 Spin Crossover System (ptz= 1-propyltetrazole). *J. Chem. Phys.* **1991**, *94*, 2741–2748.

(20) Reiher, M., Salomon, O. & Artur Hess, B. Reparameterization of Hybrid Functionals Based on Energy Differences of States of Different Multiplicity. *Theor. Chem. Acc.* **2001**, *107*, 48–55.

(21) Hirata, S. & Head-Gordon, M. Time-dependent Density Functional Theory within the Tamm-Dancoff Approximation.. *Chem. Phys. Lett.* **1999**, *314*, 291–299.

(22) Schafer, A., Huber, C. & Ahlrichs, R Fully Optimized Contracted Gaussian Basis Sets of Triple Zeta Valence Quality for Atoms Li to Kr.. *J. Chem. Phys.* **1994**, *100*, 5829–5835.

(23) Wang, F. & Ziegler, T. A Simplified Relativistic Time-Dependent Density-Functional Theory Formalism for the Calculations of Excitation Energies including Spin-Orbit Coupling Effect. *J. Chem. Phys.* **2005**, *123*, 154102.

(24) Neese, F. The ORCA Program System. *WIREs Comput Mol Sci* **2012**, *2*, 73–78.

(25) *ADF2009.01, SCM, Theoretical Chemistry, Vrije Universiteit, Amsterdam, The Netherlands* (Scientifici Computation and Modelling, **2010**). Http://www.scm.com/. .

(26) Köppel, H., Domcke, W. & Cederbaum, L. S. Multimode Molecular Dynamics Beyond the Born-Oppenheimer Approximation **1984**, *57*, 59–246.

(27) Beck, M. H., Jäckle, A., Worth, G. A. & Meyer, H.-D. The Multiconfiguration Time-Dependent Hartree method: A Highly Efficient Algorithm for Propagating Wavepackets. *Phys. Rep.* **2000**, *324*, 1–105